




Direct Numerical Simulation of a Moist Cough Flow using Eulerian Approximation for Liquid Droplets

Rohit Singhal, S. Ravichandran & Sourabh S. Diwan

To cite this article: Rohit Singhal, S. Ravichandran & Sourabh S. Diwan (2021) Direct Numerical Simulation of a Moist Cough Flow using Eulerian Approximation for Liquid Droplets, International Journal of Computational Fluid Dynamics, 35:9, 778-797, DOI: [10.1080/10618562.2022.2057479](https://doi.org/10.1080/10618562.2022.2057479)

To link to this article: <https://doi.org/10.1080/10618562.2022.2057479>

 View supplementary material 

 Published online: 24 Apr 2022.

 Submit your article to this journal 

 View related articles 

 View Crossmark data 



Direct Numerical Simulation of a Moist Cough Flow using Eulerian Approximation for Liquid Droplets

Rohit Singhal ^a, S. Ravichandran ^b and Sourabh S. Diwan ^a

^aDepartment of Aerospace Engineering, Indian Institute of Science, Bengaluru, India; ^bNordic Institute for Theoretical Physics, KTH Royal Institute of Technology and Stockholm University, Stockholm, Sweden

ABSTRACT

The COVID-19 pandemic has inspired several studies on the fluid dynamics of respiratory events. Here, we propose a computational approach in which respiratory droplets are coarse-grained into an Eulerian liquid field advected by the fluid streamlines. A direct numerical simulation is carried out for a moist cough using a closure model for space-time dependence of the evaporation time scale. Stokes-number estimates are provided, for the initial droplet size of $10\ \mu\text{m}$, which are found to be $\ll 1$, thereby justifying the neglect of droplet inertia, over the duration of the simulation. Several important features of the moist-cough flow reported in the literature using Lagrangian tracking methods have been accurately captured using our scheme. Some new results are presented, including the evaporation time for a ‘mild’ cough, a saturation-temperature diagram and a favourable correlation between the vorticity and liquid fields. The present approach can be extended for studying the long-range transmission of virus-laden droplets.

ARTICLE HISTORY

Received 4 October 2021
Accepted 14 March 2022

KEYWORDS


Direct numerical simulation; moist cough flow; respiratory droplets; liquid field approximation; thermodynamics of phase change; long-range pathogen transmission; COVID-19


1. Introduction

The airborne transmission of respiratory infection is thought to be responsible for the COVID-19 pandemic that is afflicting the world. The SARS-CoV-2 virus responsible for the contagion spreads through the air, not only by people with respiratory symptoms (coughing/sneezing) (Bourouiba 2020) but also by asymptomatic carriers through speech and even breathing (Morawska and Cao 2020). As a result, the fluid and droplet dynamics of the various respiratory events have been a subject of several investigations, especially since the start of the pandemic. These include studies on symptomatic respiratory events such as coughs or sneezes (Chong et al. 2021; Rosti et al. 2021; Fabregat et al. 2021; Domino 2021), as well as those on everyday activities like breathing, talking, or singing (Morawska et al. 2009; Chao et al. 2009; Abkarian et al. 2020; Singhal, Ravichandran, Govindarajan, et al. 2021).

Airborne transmission occurs through the transport of tiny, virus-laden liquid droplets expelled during respiratory events (Bourouiba 2021b; Mittal, Ni, and Seo 2020). These droplets vary in size

from a few micrometers to hundreds of micrometers (Duguid 1946; Somsen et al. 2020). The large droplets ($\mathcal{O}(100\text{--}1000)\ \mu\text{m}$) settle rapidly and are thus removed from the flow over distances $\mathcal{O}(1\ \text{m})$ (Bourouiba, Dehandschoewercker, and Bush 2014). (They may survive on the surfaces where they land, leading to ‘fomite’ transmission; this was believed, at the beginning of the pandemic, to be an important mode of transmission of SARS-CoV-2; see Asadi et al. 2020; Morawska and Cao 2020.) On the other hand, since small droplets remain suspended in the respiratory flow for longer times, they are transported over larger distances. The turbulence present in respiratory flows (which can be effectively modelled as turbulent puffs; Bourouiba, Dehandschoewercker, and Bush 2014) plays an important role in determining the trajectories of such droplets. Sufficiently small droplets (called aerosols) may, in fact, remain suspended and be transmitted through ventilation systems in large buildings (Qian and Li 2010; Zhao, Zhang, and Li 2005; Chen and Zhao 2010). Since the early work of Wells (1934), human respiratory

CONTACT S. S. Diwan  sdiwan@iisc.ac.in

 Supplemental data for this article can be accessed here. <https://doi.org/10.1080/10618562.2022.2057479>

flows have been studied experimentally to determine the droplet size distribution and typical flow velocities at the mouth, and the subsequent flow and droplet evolution; for more recent studies, see Abkarian et al. (2020), Bourouiba, Dehandschoewercker, and Bush (2014), Gupta, Lin, and Chen (2009) and Stadenytskyi et al. (2020). The experimental studies have also served to provide useful inputs to numerical investigations, e.g. for determining the parameters of the simulation.

Numerical studies of the dynamics of droplets over distances larger than a few metres are computationally expensive and typically utilise the Reynolds-averaged Navier–Stokes (RANS) equations which involve ad-hoc models for the turbulent viscosities and diffusivities; a typical example is the building ventilation, which involves large length and time scales ($\mathcal{O}(10\text{ m})$ and $\mathcal{O}(10^3\text{ s})$) (Qian and Li 2010; Shao et al. 2021). Similar approaches have also been used in studying the effects of nonzero ambient flow (such as the presence of wind) on the dispersion of virus-laden droplets in individual respiratory events (Dbouk and Drikakis 2020; Feng et al. 2020). Note that the individual respiratory flows that travel up to a distance of 2m are amenable to more accurate simulation methods such as large-eddy simulation (LES) and direct numerical simulation (DNS). The former resolves the large energy-carrying scales in the flow while parameterising the smaller scales (Abkarian et al. 2020; Liu et al. 2021), whereas the latter aims to resolve scales sufficiently small (ideally up to the Kolmogorov scale) so that the dissipation of energy is captured accurately (Moin and Mahesh 1998); see Chong et al. (2021) and Rosti et al. (2021). Such detailed numerical studies, combined with experimental studies, offer better insight into the survival and transmission of droplets, which may in turn help improve the respiratory-flow models in large-scale studies, such as ventilation.

Human respiratory flows are essentially multi-phase flows in which the evaporation and condensation processes play an important role in determining the droplet lifetime (Chong et al. 2021; Wells 1934). Such processes can also affect the buoyancy of the respiratory flow through the release/absorption of the latent heat. It is therefore important to incorporate the thermodynamics of phase change in a numerical simulation of such flows. However, for flows generated during a human speech, the droplets are typically

very small ($\mathcal{O}(5\text{ }\mu\text{m})$), and evaporate fast to convert into droplet nuclei in the form of dissolved solid substances which can continue to harbour virions. Such flows have been simulated without incorporating phase changes and using a scalar field to mimic the transport of the droplet nuclei (Abkarian et al. 2020; Singhal, Ravichandran, Govindarajan, et al. 2021).

On the other hand, in flows generated by violent respiratory events like coughs or sneezes, a wide range of droplet sizes is present, and there is a considerable variation in the maximum droplet size expelled during a cough or a sneeze from one person to another (Bourouiba 2021a). As a result, for such flows, the phase changes of liquid droplets into a vapour and vice-a-versa are critical for understanding the flow evolution and droplet dynamics; another relevant aspect is the gravitational settling of large droplets, typically greater than $100\text{ }\mu\text{m}$ in diameter. Recent numerical studies have investigated these aspects, including the role of turbulence on thermodynamics and droplet motion. Chong et al. (2021) performed DNS of a turbulent vapour puff and showed that the relative humidity and temperature of the ambient affect the longevity of the liquid water droplets; see also Ng et al. (2021). They carried out simulations for 50% and 90% ambient relative humidity and found the presence of supersaturation in the flow for the latter case, which promoted an initial droplet growth resulting in extended droplet lifetimes. Rosti et al. (2021) compared the results on the evolution of droplets obtained from a DNS with those obtained from a coarse-DNS (i.e. after filtering out small-scale fluctuations) and showed that the latter could considerably underestimate the lifetime of droplets. Liu et al. (2021), in their LES study, found that a portion of their simulated moist puff separated from the main flow and travelled along a random direction at a faster speed. They also proposed a theory for predicting puff size, velocity, distance travelled and droplet size distribution and compared the predictions with their LES results.

The above DNS and LES studies have employed a coupled Eulerian-Lagrangian approach to solve for the fluid and droplet velocities respectively; see also Fabregat et al. (2021). These simulations have provided a wealth of useful information and have helped enhance our understanding of the dynamics of respiratory flows. However, since this approach involves tracking each individual droplet, the data that needs to be handled can become exceedingly large, especially when

the respiratory event expels a large number of droplets of moderate size (which can be as large as 10^5 droplets per cm^3 ; Bourouiba 2021a). This also makes such simulations computationally expensive, inherently limiting their use in numerical experiments and parametric studies. In this work, we use a middle ground between the Lagrangian particle tracking methods, and RANS simulations, by coarse-graining the liquid water droplets into an Eulerian field that is carried with the flow, while resolving sufficiently small scales in the flow. This approach, in principle, solves for only one of the moments of the droplet distribution—the total liquid content—in the flow, and is familiar in the atmospheric sciences as the ‘one-moment’ scheme (e.g. Lin, Farley, and Orville 1983; Grabowski 1998; see Beck and Watkins (2002), which discusses the relevance of this method for analysing dense liquid sprays). Here we propose an ‘extended one-moment’ scheme in which we interpret the liquid field in terms of a collection of droplets with the number density considered uniform in space (but varying in time), and the droplet radius a function of space and time. Since we resolve the small scales in the flow, the computational requirements remain much greater than that for RANS simulations of the same problem. However, our approach is algorithmically simpler than Lagrangian particle tracking while still solving the Navier–Stokes equations without modelling approximations.

We use this approach to study the typical flow produced by a ‘mild’ cough, i.e. involving relatively low cough flow rates as in a ‘throat-clearing’ cough, for example. The Navier–Stokes equation is solved within the Boussinesq approximation and the Clausius–Clayperon relation is used for relating local relative humidity to local temperature. The extended one-moment scheme provides a closure for the evaporation/condensation rates in the flow. The liquid content at the orifice (which mimics mouth opening) is prescribed to be consisting of an initially mono-disperse distribution of droplets with $10\ \mu\text{m}$ of diameter, which is small enough to neglect droplet inertia. This assumption is supported *a posteriori* by providing estimates of the Stokes number which are shown to be much smaller than unity. We carry out a careful comparison of our results with those from the literature obtained using Lagrangian particle tracking and show that we are able to reproduce many of the important features of a moist cough flow, including the initial supersaturation. We also present some new results on

the relative rates of decay of the saturation and temperature fields away from the orifice, and the interplay between the liquid content and vorticity fields.

The remainder of the paper is organised as follows. We describe the geometry of the problem and the governing evolution equations in Section 2, including the treatment for incorporating the thermodynamics of phase change. Therein, we also provide numerical details for the present simulation. Section 3 reports simulation results wherein we first compare the results from the extended one-moment scheme with a more rudimentary model of treating evaporation time scale as a constant. This is followed by a detailed analysis of the data *vis-a-vis* available results. We end Section 3 by presenting some thoughts on the advantages/limitations of the proposed approach in the context of respiratory flows. Finally, the conclusions are presented in Section 4.

2. Governing Equations and Numerical Details

2.1. Geometry and Problem Setup

The domain used in the present numerical simulations, shown schematically in Figure 1(a), is a cuboidal volume of dimensions $L_x \times L_y \times L_z$. Here x , y and z are the axial, vertical (against gravity) and lateral co-ordinates respectively. Following Gupta, Lin, and Chen (2009), the mouth of the person coughing is modelled as a circular orifice with a diameter $d_o = 2.25\text{cm}$ in the vertical y – z plane, and is centred at the origin of coordinates (Figure 1(a)). The inlet velocity u_0 at the orifice is obtained from the laboratory measurements of the flow rates in cough flows reported in Gupta, Lin, and Chen (2009) (see Figure 5 in Gupta, Lin, and Chen 2009).

Two quantities specify the flow-rate profile as a function of time at the orifice – (a) the maximum flow rate or the cough peak flow rate (CPFR) and (b) the time of its occurrence or the peak-velocity time (PVT). A wide range of values have been reported for CPFR (1.6–8.5 l/s) and PVT (0.057–0.11 s); see Gupta, Lin, and Chen (2009). Here we choose CPFR = 3.0 l/s and PVT = 0.06 s representative of a ‘mild’ cough, and the resulting flow rate as a function of time is shown in Figure 1(b). The total volume of fluid expelled from the orifice, the cough expiratory volume (V_o), is 0.679 l in a total cough time of 0.528 s; V_o is the integral under the curve in Figure 1(b). The average velocity based on

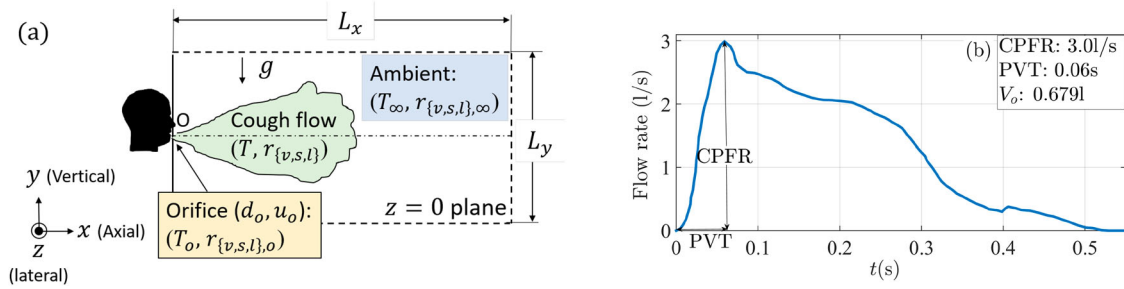


Figure 1. (a) A Schematic side view ($z = 0$) of the computational domain used to simulate a mild cough. A jet of velocity $u_o(t)$ exits the mouth, modelled as an orifice of diameter d_o . The temperature T and the mixing ratios of the vapour and liquid $r_{v,l}$ at the orifice (subscript o) and the ambient (subscript ∞) are specified. (b) The prescribed flow rate at the orifice used to calculate the inlet velocity u_o at the orifice.

the orifice flow rate and total cough time is taken as the characteristic velocity scale, $u_c = 3.232$ m/s.

Since we consider the thermodynamics of evaporation of the liquid droplets expelled during a cough, the temperature and other thermodynamic variables at the orifice and in the ambient need to be specified. We label quantities at the orifice with a subscript o and ambient quantities with a subscript ∞ (see Figure 1(a)). We set the orifice temperature $T_o = 34^\circ\text{C}$ to a value slightly lower than the typical body temperature and set the ambient temperature to a typical indoor temperature of $T_\infty = 20^\circ\text{C}$. These conditions are the same as those used by Chong et al. (2021); see also Bourouiba, Dehandschoewercker, and Bush (2014). We use T_∞ and $\Delta T_o = T_o - T_\infty$ as the characteristic scales respectively for temperature and temperature difference. The survival time of exhaled droplets increases as the temperature difference between the exhaled cough fluid and ambient indoor air, typically positive, increases (Chong et al. 2021), with other parameters kept constant.

In addition to liquid droplets of a range of sizes, the exhaled fluid in a cough also contains water vapour, both mixed with dry air. The amount of water substance in a cough is typically a small fraction by mass of the (dry) air (10^{-5} – 10^{-7} ; Bourouiba, Dehandschoewercker, and Bush 2014). We define the mixing ratios (mass per unit mass of dry air) of vapour as $r_v = \rho_v/\rho_d$ and liquid as $r_l = \rho_l/\rho_d$, where ρ_d , ρ_v and ρ_l are the densities of dry air, vapour and liquid water respectively. (We do not model the viscoelastic nature of the saliva droplets or the dissolved solid substances in these droplets.) The values of r_v are more conveniently expressed in terms of the relative humidity $s = r_v/r_s$, where r_s is the saturation vapour mixing ratio. For the present simulations, the humidity conditions are

assigned as $s_\infty = 0.9$ for the ambient, and $s_o = 1$ at the orifice. These values are chosen so as to replicate one of the cases in Chong et al. (2021), who have used s of 0.5 and 0.9 for the ambient and 1 for the orifice. This enables comparison of our results (especially the condensational growth due to supersaturation) obtained within the Eulerian field approximation with those in Chong et al. (2021) who have done Lagrangian tracking of individual liquid droplets. Furthermore, r_v and r_l are also normalised using the saturation mixing ratio of the ambient, $r_{s,\infty}$ as the characteristic scale. We next describe the assumptions underlying the coarsening of the liquid water droplets into an Eulerian field.

2.2. Eulerian Treatment of Droplets

Human coughs produce droplets of a wide range of sizes – a commonly used distribution is the one provided by Duguid (1946), which ranges from ($2\ \mu\text{m}$ – $1\ \text{mm}$); see Chong et al. (2021), Rosti et al. (2021) and Bourouiba, Dehandschoewercker, and Bush (2014). However, it is important to realise that no two coughs are identical, and many different droplet-size distributions obtained from laboratory experiments on human subjects have been reported in the literature. Bourouiba (2021a) has compiled the available data, which shows that coughs can have droplet concentrations as low as $0.1\ \text{cm}^{-3}$ and as high as $10^5\ \text{cm}^{-3}$, with the maximum droplet sizes ranging from $5\ \mu\text{m}$ to $1\ \text{mm}$. Droplets of finite size have velocities that are, in general, different from the velocity of the carrier fluid in which they are suspended. Large droplets (diameters $> 100\ \mu\text{m}$) are dominated by gravity and undergo rapid sedimentation within range of $\sim 1\ \text{m}$ (Chong et al. 2021; Bourouiba, Dehandschoewercker,

and Bush 2014). Droplets less than $100 \mu\text{m}$ in size are carried away by the flow over longer distances before they settle down (Bourouiba 2021b). As the droplet size reduces, the response time of the droplet (τ_p) gets smaller in comparison with the typical flow time (τ_f). This effect is quantified by the Stokes number $St = \tau_p/\tau_f$, which indicates how important the inertial effects are for a given droplet size. For droplets with small Stokes numbers (typically less than $50 \mu\text{m}$ in diameter), it may be possible to coarse-grain them in the form of an Eulerian field for the liquid content (i.e. $r_l = r_l(x, y, z, t)$), while still retaining the inertial effects (Ravichandran, Meiburg, and Govindarajan 2020; Ravichandran and Narasimha 2020). This, in essence, is the Eulerian approximation for liquid droplets, which we use in this work. Such an approximation is commonly known as the one-moment scheme in the atmospheric cloud literature (see, e.g. Ravichandran, Meiburg, and Govindarajan 2020; Ravichandran and Narasimha 2020). When the inertial effects are retained, the velocity field of the droplets is not divergence-free, but obeys a compressible advection equation. The time rate of change of the liquid water mixing ratio, r_l , within this framework, can be written:

$$\frac{dr_l}{dt} \equiv C_d = \frac{\partial r_l}{\partial t} + \nabla \cdot (vr_l), \quad (1)$$

where, C_d is condensation rate. The droplet velocity field ($v(t)$) can be written down using the Maxey-Riley equation (Maxey and Riley 1983), which governs the dynamics of particles in the Stokes regime:

$$\frac{dv}{dt} = \frac{\mathbf{u} - \mathbf{v}}{\tau_p} + \mathbf{g}, \quad (2)$$

where the droplets are assumed to be much denser than air, \mathbf{g} is gravitational acceleration, and \mathbf{u} is flow velocity. For small droplets, Equation (2) may be expanded in powers of τ_p to give, to first order,

$$\mathbf{v} = \mathbf{u} - \tau_p \frac{D\mathbf{u}}{Dt} + \tau_p \mathbf{g}, \quad (3)$$

where D/Dt is the material derivative following fluid streamlines, and $\tau_p \mathbf{g}$ is the terminal Stokes velocity for the droplet. Equation (3) can be written in non-dimensional form (choosing appropriate flow velocity

and length scales) as

$$\tilde{\mathbf{v}} = \tilde{\mathbf{u}} - St \frac{D\tilde{\mathbf{u}}}{D\tilde{t}} + St \tilde{\mathbf{g}} + \mathcal{O}(St^2), \quad (4)$$

where $\tilde{\cdot}$ indicates a non-dimensional quantity. In the current study, we consider the liquid content at the orifice to represent an initial mono-disperse collection of N_o number of droplets of diameter $10 \mu\text{m}$. This diameter is sufficiently small to expect the inertial effects to be negligible, at least for the short-range aerosol transmission. Moreover, typical human coughs consist of a large number of droplets within the size range of $10\text{--}30 \mu\text{m}$ (Zayas et al. 2012; Hersen et al. 2008; Lindsley et al. 2013; Yang et al. 2007), including some cases wherein the maximum droplet size is about $10 \mu\text{m}$ as mentioned earlier (Bourouiba 2021a). Also this is the size range that is responsible for the long-range transport of pathogens contributing to airborne transmission (Rosti et al. 2021; Ng et al. 2021). We, therefore, choose droplets of size $10 \mu\text{m}$, and assume that the effect of the ‘slip’ velocity between the droplets and the carrier fluid can be neglected so that the droplets effectively follow the fluid streamlines, i.e. $\tilde{\mathbf{v}} = \tilde{\mathbf{u}}$ in Equation (4). (See a discussion in Abkarian et al. (2020) and Singhal, Ravichandran, Govindarajan, et al. (2021) on this aspect with respect to speech flows.) We justify this assumption *a posteriori* by computing the Stokes numbers of the droplets as a function of space and time and show them to be sufficiently small (see Figure 6). Furthermore, we have carried out an assessment of the behaviour of the Stokes drag and gravitational settling terms (i.e. second and third terms on the right-hand side of Equation (4)) based on the simulation results, which is presented in section S5 of the supplementary material. We show that the Stokes drag term $St D\tilde{\mathbf{u}}/D\tilde{t}$ decreases continuously with time and can be neglected in the limit $St \rightarrow 0$. On the other hand, the non-dimensional gravity term $\tilde{\mathbf{g}}$ increases continuously with time and the gravitational settling velocity can be expected to become comparable with fluid velocity in the long-time limit (i.e. for simulation times of tens of seconds or longer) in the absence of background ventilation. For the short-time evolution of cough flow (such as $t = 6 \text{ s}$ as done here), the gravitational settling term is an order of magnitude smaller than fluid velocity and its neglect is therefore justified; see Section 3.3 for further comments on this point. For the present simulations, we take the total amount of liquid expelled during the cough to

Table 1. Physical properties used in the present study.

Latent heat of vapourisation of water	L_v	2.4×10^6 J/kg
Gas constant for water vapour	R_v	462 J/K kg
Density of liquid water	ρ_w	1000 kg m ⁻³
Density of dry air	ρ_d	1.2 kg m ⁻³
Kinematic viscosity of air	ν	1.5×10^{-5} m ² s ⁻¹
Acceleration due to gravity	g	9.81 m s ⁻²
Saturation vapour mixing ratio at orifice	$r_{s,o}$	3.47×10^{-2} kg/kg of dry air
Saturation vapour mixing ratio in ambient	$r_{s,\infty}$	1.47×10^{-2} kg/kg of dry air

be $10 \mu\text{l}$ (Duguid 1946), giving $N_o = 1.91 \times 10^7$ (i.e. with droplet concentration of $2.8 \times 10^4 \text{ cm}^{-3}$). For the total cough volume of 0.679 l, the initial volume fraction of liquid water is 1.47×10^{-5} , which translates into a liquid mixing ratio at the orifice of $r_{l,o} \approx 1.23 \times 10^{-2}$ kg/kg of dry air. During the cough (which lasts for 0.528 s), the instantaneous liquid amount expelled from the orifice is taken to be proportional to the cough velocity at that time (Figure 1(b)).

2.3. Thermodynamics of Phase Change

The mixing ratios of vapour and liquid water are coupled to the local temperature through the Clausius-Clapeyron law which specifies the saturation mixing ratio of vapour (r_s) at a given local temperature:

$$r_s(T) = r_{s,\infty} \exp\left(\frac{L_v}{R_v} \left(\frac{1}{T_\infty} - \frac{1}{T}\right)\right), \quad (5)$$

where $r_{s,\infty}$ is the saturation mixing ratio of the ambient (see, e.g. Murphy and Koop 2005), L_v is the latent heat of vapourisation of water, and R_v is the gas constant for water vapour. The values for the various physical constants used in this simulation are given in Table 1. As $\epsilon = \Delta T_o/T_\infty = 14/293 \equiv \mathcal{O}(10^{-2})$, we approximate the exponent in equation (5) as $L_v(1/T_\infty - 1/T)/R_v = L_v(T - T_\infty)/R_v T_\infty^2$; see Ravichandran and Narasimha (2020).

The saturation mixing ratio r_s is the amount of vapour r_v that can exist in equilibrium at a given temperature. In saturated parcels with $r_v > r_s$, the vapour condenses into liquid water. Conversely, the liquid water in parcels with $r_v < r_s$ evaporates. In the following, we first provide a treatment for the thermodynamics of phase change for a collection of droplets and then suggest two closure models that we have used for thermodynamics of the Eulerian liquid field.

For liquid droplets (which act as nuclei for condensation), the condensation and evaporation processes occur on a timescale that depends on their numbers and sizes. Note that we have implicitly assumed that the ambient has no other nuclei for condensation. The condensation rate C_d can be written as

$$C_d \equiv \frac{dr_l}{dt} = n \cdot 4\pi a^2 \frac{da}{dt} \cdot \frac{\rho_w}{\rho_d}, \quad (6)$$

where a and ρ_w are droplet radius and the density of liquid water, respectively, and n is the droplet density, i.e. number of droplets per unit cough volume. For isolated droplets growing by vapour diffusion, the droplet growth rate is given by (see, e.g. Bohren and Albrecht 2000)

$$a \frac{da}{dt} = \frac{1}{C\rho_w} \left(\frac{r_v}{r_s} - 1\right), \quad (7)$$

where $C \approx 10^7 \text{ ms kg}^{-1}$ is a weak function of temperature (Ravichandran and Narasimha 2020). The factor $r_v/r_s - 1$ is the ‘supersaturation’; for $r_v < r_s$, this factor is negative and the droplets shrink by evaporation. Using equation (7) in equation (6), and introducing non-dimensionalisation, we get

$$\frac{d\tilde{r}_l}{d\tilde{t}} = \frac{\mathcal{H}}{\tilde{\tau}_c} \left(\frac{\tilde{r}_v}{\tilde{r}_s} - 1\right), \quad (8)$$

where the phase change time scale

$$\tilde{\tau}_c = \frac{u_c C \rho_d r_{s,\infty}}{d_c 4\pi a n} \quad (9)$$

accounts for the surface area of droplets available for evaporation, and the modified Heaviside function is given by

$$\mathcal{H} = \begin{cases} 1 & \text{if } r_v > r_s \text{ or } r_l > 0 \\ 0 & \text{otherwise.} \end{cases} \quad (10)$$

Here, $\tilde{\tau}_c$ is an important parameter that tunes the rate of condensation/evaporation at any given saturation condition and d_c is the characteristic length scale ($= d_o$; Figure 1(a)). Note that the quantities a and n appearing in the equation for $\tilde{\tau}_c$ (Equation (9)) cannot, by definition, be independently determined in a one-moment scheme and therefore further modelling needs to be done. Here we use the following two models for $\tilde{\tau}_c$, which depend upon how the Eulerian liquid field is interpreted in terms of droplets.

In the first model, we determine $\tilde{\tau}_c$ at the beginning of the cough (at $t = 0$ s) and treat it as constant throughout the simulation (denoted as ‘const. τ ’). This approach is typically used in cumulus cloud studies where $\tilde{\tau}_c$ is small and is of $\mathcal{O}(0.1)$ (Ravichandran, Meiburg, and Govindarajan 2020; Hernandez-Duenas et al. 2013). For the present cough flow problem, based on the initial diameter of droplets $D_o = 2a_o = 10 \mu\text{m}$ and initial droplet density $n_o = N_o/V_o$, $\tilde{\tau}_c$ comes out to be 14.34. This is much larger than that in clouds which is primarily due to the much smaller width of the cough flow in comparison to that of a cumulus cloud. As a result, using a constant $\tilde{\tau}_c$ for a cough flow is strictly not justified. Here we use it to provide a baseline case for comparison with the second model for $\tilde{\tau}_c$ explained below.

In the second model, we allow $\tilde{\tau}_c$ to be variable. Ravichandran, Meiburg, and Govindarajan (2020) used a variable $\tilde{\tau}_c$ model for computing mammatus cloud evolution, in which the number density was assumed constant in time and the droplet radius (considered initially mono-disperse) decreased as a function of time. Here we extend this treatment by noting that as the cough volume increases due to continued entrainment, the droplet number density goes on decreasing with time. Secondly, since the liquid content r_l is a function of space and time, the product $n \times a^3$ is essentially a function of space and time (Equation (12)). Due to the limitation of the Eulerian approximation for liquid droplets, we cannot determine both n and a as functions of space and time. In what follows, we will consider the number density to be a function of t and the droplet radius to be a function of x, y, z and t . This model, which represents an ‘extended’ first-order moment scheme, will be denoted as ‘var. τ ’ and is based on the following two considerations.

- (1) Although the droplets released from the orifice are mono-disperse initially, they are subjected to different saturation fields within the cough volume (as will be shown below). As a result, one can expect the resulting droplet distribution to be poly-disperse. For example, Rosti et al. (2021) have carried out a simulation with an initial mono-disperse droplet distribution at the orifice and observed a considerable broadening of the evaporation time caused

by turbulence, implying the presence of different droplet sizes.

- (2) Since we do not consider inertial effects for liquid droplets (or liquid field), the preferential clustering of droplets will not be present (Monchaux, Bourgoin, and Cartellier 2012; Yoshimoto and Goto 2007). There can still be some concentration and dilution of liquid field as the instantaneous fluid streamlines come closer or diverge. But this effect is expected to be much weaker than the inertial clustering. It is, therefore, reasonable to consider an ‘effectively uniform’ distribution of droplets so that the number density is only a function of time. One may also consider this as an ‘equivalent’ uniform distribution of droplets that enables (approximately) characterising the liquid field within the cough volume as a poly-disperse distribution of droplets (considered in point 1 above).

With these considerations, the local value of $\tilde{\tau}_c(\mathbf{x}, t)$ may be written as

$$\tilde{\tau}_c(\mathbf{x}, t) = \frac{u_c}{d_c} \frac{C\rho_d r_{s,\infty}}{4\pi a(\mathbf{x}, t)n(t)}, \quad (11)$$

where $a(\mathbf{x}, t)$ is the local droplet radius given implicitly from the definition of r_l as

$$\rho_d r_l(\mathbf{x}, t) = \frac{4\pi}{3} n(t) a^3(\mathbf{x}, t) \rho_w, \quad (12)$$

and $n(t)$ is given by

$$n(t) = N(t)/V(t). \quad (13)$$

The total number of droplets (including liquid droplets and droplet nuclei) in the cough volume, $N(t) = N_o$ for $t > t_o = 0.528$ s. For $t < t_o$, $N(t)$ is taken to be proportional to the fluid volume expelled ($= \int_0^t$ ‘cough flow-rate’ dt) at the origin up to time t . $V(t)$ is the volume of cough at time t and is determined based on a threshold for the cough-flow presented in Section 3. The evaporation model used in the solver has been validated against the standard case of a collection of droplets evaporating in stationary air (not shown here).

2.4. Governing Equations

As the flow velocities and the temperature differences in the flow are small, we make the Boussinesq approximation, with density differences appearing only in the buoyancy term. This approximation has been used in the recent DNS and LES studies on cough and speech flows (Chong et al. 2021; Rosti et al. 2021; Abkarian et al. 2020; Singhal, Ravichandran, Govindarajan, et al. 2021). The equations governing the dynamics are thus the incompressible Navier–Stokes equations for the velocity, coupled with scalar equations for the temperature and mixing ratios of vapour and liquid water with appropriate source/sink terms for the scalars.

$$\nabla \cdot \mathbf{u} = 0; \quad (14)$$

$$\frac{D\mathbf{u}}{Dt} = -\frac{\nabla p}{\rho_\infty} + \nu \nabla^2 \mathbf{u} + \mathbf{B}; \quad (15)$$

$$C_p \frac{D\theta}{Dt} = \kappa \nabla^2 \theta + L_v C_d; \quad (16)$$

$$\frac{Dr_v}{Dt} = \kappa_v \nabla^2 r_v - C_d; \quad (17)$$

$$\frac{Dr_l}{Dt} = \kappa_l \nabla^2 r_l + C_d. \quad (18)$$

Here, ν is the fluid viscosity of air, κ , κ_v and κ_l are the diffusivities of temperature, vapour and liquid, respectively, L_v is the latent heat of vaporisation of water, and $\theta = T - T_\infty$ is the temperature difference. The buoyancy term, obtained within the Boussinesq approximation, is given by,

$$\begin{aligned} \mathbf{B} &= g \frac{\rho_\infty - \rho}{\rho_\infty} \hat{e}_y = g \\ &\times \left[\frac{T - T_\infty}{T_\infty} + (\xi - 1)(r_v - r_{v,\infty}) - r_l \right] \hat{e}_y, \end{aligned} \quad (19)$$

where ξ ($= 1.61$) is the ratio of gas constants of air and water vapour. This is obtained by writing $\rho = \rho_d(1 + r_v + r_l)$ and $\rho_\infty = \rho_{d,\infty}(1 + r_{v,\infty})$, and by performing a linearisation for small magnitudes of r_l and r_v . A detailed derivation of Equation (19) can be found in Ravichandran and Narasimha (2020).

Equations (14)–(18) are non-dimensionalised using the length scale d_c ($= d_o$), the velocity scale u_c , the temperature scale ΔT_o , and the scale for water mixing ratios $r_{s,\infty}$, giving the non-dimensional governing equations

$$\tilde{\nabla} \cdot \tilde{\mathbf{u}} = 0, \quad (20)$$

$$\begin{aligned} \frac{D\tilde{\mathbf{u}}}{D\tilde{t}} &= -\tilde{\nabla}\tilde{p} + \frac{1}{Re} \tilde{\nabla}^2 \tilde{\mathbf{u}} + \frac{1}{Fr^2} \\ &\times \left[\tilde{\theta} + \frac{r_{s,\infty}}{\epsilon} ((\xi - 1)(\tilde{r}_v - \tilde{r}_{v,\infty}) - \tilde{r}_l) \right] \hat{e}_y, \end{aligned} \quad (21)$$

$$\frac{D\tilde{\theta}}{D\tilde{t}} = \frac{1}{RePr} \tilde{\nabla}^2 \tilde{\theta} + L_1 \tilde{C}_d, \quad (22)$$

$$\frac{D\tilde{r}_v}{D\tilde{t}} = \frac{1}{ReSc_v} \tilde{\nabla}^2 \tilde{r}_v - \tilde{C}_d, \quad (23)$$

$$\frac{D\tilde{r}_l}{D\tilde{t}} = \frac{1}{ReSc_l} \tilde{\nabla}^2 \tilde{r}_l + \tilde{C}_d, \quad (24)$$

where the Reynolds number $Re = d_c u_c / \nu = 4849$, the inverse-square Froude number $Fr^{-2} = g \epsilon d_c / u_c^2 = 1.01 \times 10^{-3}$, the Prandtl number $Pr = 0.71$, the Schmidt numbers $Sc_{v,l} = 1$, and the non-dimensional latent heat of vaporisation

$$L_1 = \frac{L_v r_{s,\infty}}{C_p T_\infty \epsilon} = 2.73. \quad (25)$$

In the above Equations (20)–(24), all the variables with $\tilde{\cdot}$ represent normalised quantities of their respective parameters, for example, $\tilde{\mathbf{u}}$ represents the normalised velocity vector. The saturation vapour mixing ratio in Equation (5) is also normalised and will be used in a form given as,

$$\tilde{r}_s(\tilde{\theta}) = \exp(L_2 \tilde{\theta}), \quad (26)$$

where non-dimensional constant L_2 is,

$$L_2 = \frac{L_v \epsilon}{R_v T_\infty}. \quad (27)$$

2.5. Numerical Method and Code Validation

Equations (20)–(24) are solved in a cuboidal domain of dimensions $80d_o$ ($= 1.8$ m in x -direction) $\times 40d_o \times 40d_o$ using the finite-volume solver *Megha-5*, which is second-order accurate in space and time. The domain is discretised with uniform and equal grid spacing (Δ) in all three directions, with a total of $1024 \times 512 \times 512$ grid points. The grid resolution in the present study is found to be as good as or better than that reported in the literature on cough-flow DNS (Chong et al. 2021; Rosti et al. 2021); see section S1 in the supplementary material. A second-order Adams-Bashforth scheme is used for time-stepping, with a CFL number of 0.15. Convective boundary conditions are imposed on all flow variables at the $x = L_x$, $y = \pm L_y/2$ and

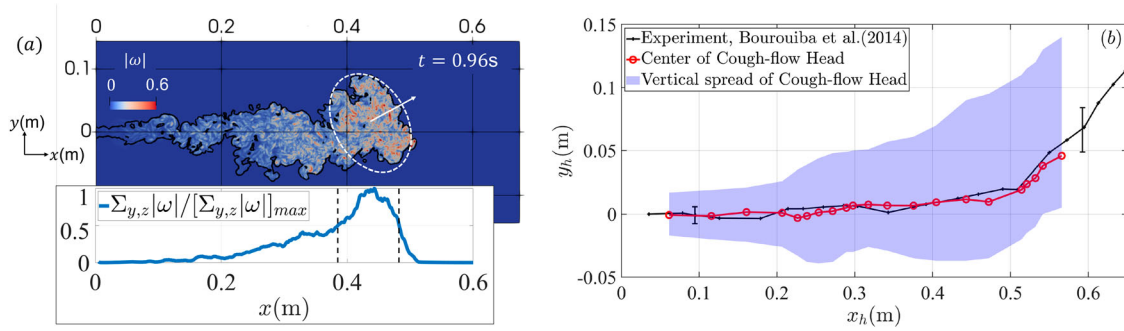


Figure 2. (a) A slice through the $z = 0$ plane at $t = 0.96$ s after the flow initiation, showing vorticity magnitude $|\omega|$ bounded by a contour line (in black) corresponding to the density difference of 1% of the value at the orifice. The white dashed circle representing the ‘head’ of the cough flow is drawn with a centre decided based on the vorticity magnitude (see the adjoining text). The inset shows the normalised distribution of $|\omega|$ summed over y - z planes, which is used to locate the x coordinate of the cough-flow head. (b) The trajectory of the centre of the cough-flow head compared with the cough-flow trajectory from the experimental measurements of Bourouiba, Dehandschoewercker, and Bush (2014) (see their Figure 11). The purple semi-transparent region indicates the vertical spread of the present cough-flow head. The error-bar reported in Bourouiba, Dehandschoewercker, and Bush (2014) is also included.

$z = \pm L_z/2$ boundaries (see Figure 1(a)). A free-slip, no penetration boundary condition on the velocity, and zero-flux boundary conditions on the scalars are imposed at $x = 0$, except for the orifice where Dirichlet boundary conditions are specified. The solver has been extensively validated and has previously been used to study the statistics of steady jets & plumes (Singhal, Ravichandran, Diwan, et al. 2021), cumulus & mammatus clouds (Ravichandran, Meiburg, and Govindarajan 2020), as well as previous studies of virus transmission by respiratory flows (Singhal, Ravichandran, Govindarajan, et al. 2021; Diwan et al. 2020). Each of the present simulated cases was run on the CRAY supercomputer (CRAY XC40) using 2048 cores and the total run time $\approx 43,000$ core-hours.

As a further validation test, we simulate the ‘dry’ cough case (i.e. a puff which is lighter than the ambient but does not contain evaporating water droplets), with the experimental results from Bourouiba, Dehandschoewercker, and Bush (2014) for ‘Case I’ in their experiment (see Table 1 in Bourouiba, Dehandschoewercker, and Bush 2014). In this experimental case, Bourouiba, Dehandschoewercker, and Bush (2014) injected saline payload of 88 cm^3 in a water tank with a density difference of $3.15 \times 10^{-3} \text{ g/cm}^3$, treated as a buoyancy scalar which under Boussinesq approximation acts as a source term for the vertical velocity; the fluid velocity at the orifice was kept approximately constant during the release of payload. We have replicated these conditions in our simulation for comparison.

The simulated dry-cough flow at time $t = 0.96$ s, visualised by contours of the vorticity magnitude

$|\omega| (= \sqrt{\omega_x^2 + \omega_y^2 + \omega_z^2})$ and an iso-surface of density difference, is shown in Figure 2(a). The ‘head’ of the cough flow at a given time instant is determined as follows. To obtain the x co-ordinate of the centre of the head (x_h), the vorticity magnitude is summed over the y - z plane ($\sum_{y,z} |\omega|$) and the resulting distribution as function of x is shown in the inset in Figure 2(a); x_h is taken to be the x co-ordinate corresponding to the maximum value of $\sum_{y,z} |\omega|$. To determine the y co-ordinate of the cough-head centre (y_h), $\sum_{x,z} |\omega|$ is calculated as a function of y , where the sum over x is carried out in the immediate vicinity of x_h (bounded by x locations at which $\sum_{y,z} |\omega|$ reaches 50% of its peak value, shown as dashed lines in the inset in Figure 2(a)). y_h is then calculated as the vorticity-weighted y co-ordinate, i.e. $y_h = \frac{\sum_y [y \cdot \sum_{x,z} |\omega|]}{\sum_y [\sum_{x,z} |\omega|]}$. The centre of the cough-flow is marked in Figure 2(a) and its trajectory in time is shown in Figure 2(b). The present cough-head trajectory is compared with the experimental result of Bourouiba, Dehandschoewercker, and Bush (2014), and the two results can be seen to agree well. The purple semi-transparent region indicates the vertical spread of the simulated cough-flow head, determined as the vertical region occupied by 90% of the total vorticity in the axial vicinity of x_h at a given time instant; Figure 2(a). To get a visual feel for the position of the cough-flow head, we have marked the head visually using the best-described shape for a puff or thermal, an ellipsoid (Scorer 1957); this is also done in Bourouiba, Dehandschoewercker, and Bush (2014). The dashed

ellipsoid in Figure 2(a) coincides with the centre of the head and is the smallest ellipsoid enveloping the vortical region under consideration.

3. Results

Here, we present simulation results for the mild cough flow described in Section 2.1 using the Eulerian models detailed in Section 2.3. We first discuss how the closure assumption of uniform (in space) number density of droplets, Equation (11), affects the dynamics in ‘var. τ ’ model and compare the results between the two models. In order to specify the droplet number density in Equation (11) for the var. τ model, the volume of the cough $V(t)$ at each time instant needs to be defined in a self-consistent manner; i.e. the turbulent puff with a complex boundary has to be delineated from the ambient. We define the cough volume as the volume of the flow with vapour mixing ratio larger than a chosen threshold. Once $V(t)$ is determined at a given time instant, $n(t)$ can be calculated from Equation (13) and $a(x, t)$ (droplet radius) from Equation (12), from which $\tilde{\tau}_c$ is obtained (Equation (11)). This enables calculating the condensation/evaporation rate $\tilde{C}_d(t)$ which is used to solve the equations for the next time instant (Equations (22)–(24)). Thus the threshold used for determining $V(t)$ needs to be ‘pre-set’ into the code for marching the solution in time.

Figure 3(a) shows an instantaneous distribution of \tilde{r}_v with two different line contours corresponding to the thresholds of $\tilde{r}_v = 0.905$ and $\tilde{r}_v = 0.91$. As can be seen, both the thresholds are effective in delineating the cough flow from the ambient. The cough volumes calculated based on these two thresholds are plotted as a function of time in Figure 3(b). There is a considerable increase in $V(t)$ with time compared to the orifice cough volume of 0.679 l; this is due to the turbulent entrainment of the ambient fluid into the cough flow (Diwan et al. 2020). At a given time instant, $V(t)$ for the threshold of $\tilde{r}_v = 0.905$ is larger than that for $\tilde{r}_v = 0.91$ as expected, and the difference between them increases to about 15% after 6 s (Figure 3(b)). Thus the precise choice of the threshold will affect the droplet number density (Equation (13)) and therefore the value of $\tilde{\tau}_c$. However, for a given r_l , an increase (decrease) in the number density (due to a different choice of the threshold) causes a decrease (increase) in the droplet radii (Equation (12)), which has a compensating effect for the determination of $\tilde{\tau}_c$ (Equation (11)). As a result,

the thermodynamic quantities like the total liquid content and the net evaporation rate do not show much difference with a change in the threshold value; see section S2 in the supplementary material for more details. This situation is entirely acceptable considering the scope of the var. τ model, which is supported by a good comparison of our results (presented below) with the available literature. In what follows, we choose a threshold of $\tilde{r}_v = 0.91$. Note that the cough volume follows a $V(t) \sim t^{3/4}$ variation over a certain time interval for both the values of threshold as seen in Figure 3(b), consistent with the previous results (see, e.g. Rosti et al. 2021). Since the $t^{3/4}$ scaling is strictly valid for a dry puff (Kovaszny, Fujita, and Lee 1975), it is expected to hold for the present cough flow (which is moist) only approximately.

3.1. Comparison of Results between the Two Models for $\tilde{\tau}_c$

We start by comparing broad features of the cough flow for the const. τ and var. τ models. The mean velocity of the cough flow (u_{mean}) and its streamwise extent (x_c) are plotted in Figure 4(a) for the two models. u_{mean} is calculated by averaging the streamwise component of velocity over the cough volume $V(t)$ at a given time instant and x_c is determined as the farthest point from the orifice where $\tilde{r}_v > 0.91$. The exhaled total momentum of the cough flow in the streamwise direction can be expected to be approximately constant. Therefore, the cough-flow velocity should decrease with time following $t^{-3/4}$, as the puff volume increases with the power law $t^{3/4}$ (Figure 3(b)). Figure 4(a) shows that the mean cough-flow velocity follows the $t^{-3/4}$ relation well, for both the models. The streamwise extent or ‘reach’ of the cough flow is another important parameter, as it determines how far droplets from an infected person can potentially transmit the virus. As seen from Figure 4(a), x_c follows the $t^{1/4}$ variation (i.e. cube-root of $V(t)$) well for the var. τ model, whereas the const. τ model shows a continuous departure from this law as time increases. This is seen more clearly in the linear graph for x_c shown in Figure 4(b), wherein the const. τ model is seen to depart from the $t^{1/4}$ variation for $t > 2$ s. Interestingly, this departure for the const. τ model is related to the size and behaviour of a chunk of the cough-flow, which separates from the main flow near its head. This feature will be discussed in relation to Figure 10(a);

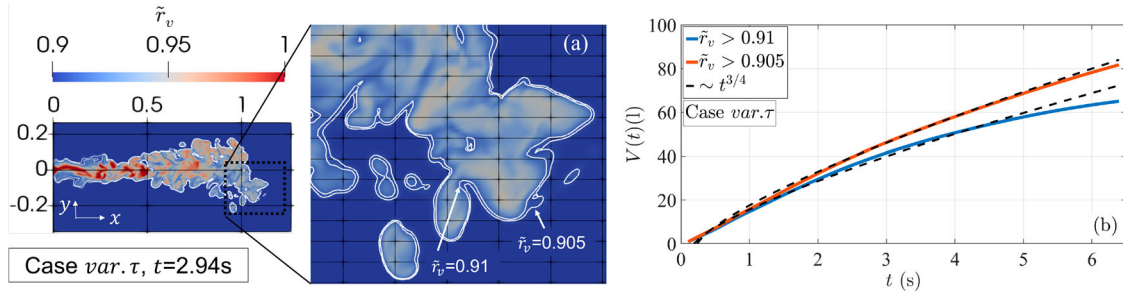


Figure 3. (a) Filled contours for the vapour mixing ratio \tilde{r}_v overlaid with line contours (in white) corresponding to $\tilde{r}_v = 0.905$ and $\tilde{r}_v = 0.91$ in the vertical ($z = 0$) plane. The inset shows a zoomed-in view at the location indicated, showing that the line contours do not change significantly as the threshold value is changed. (b) Cough volume $V(t)$ based on the two thresholds shown in (a); $V(t)$ variation approximately obeys the $3/4$ scaling for a turbulent puff.

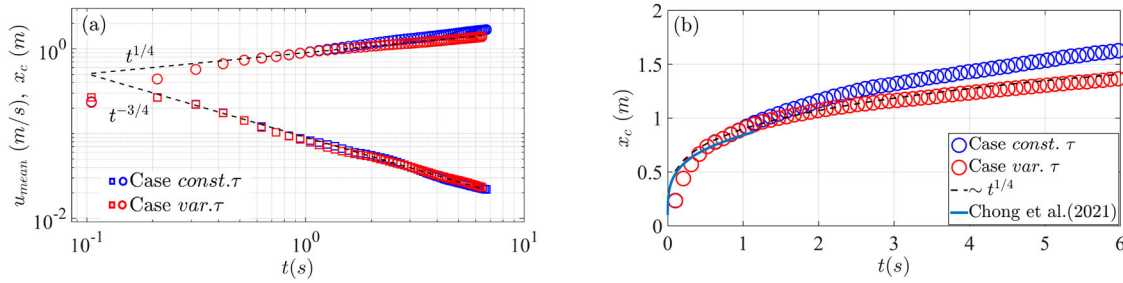


Figure 4. (a) Mean velocity u_{mean} (squares) and streamwise extent (or horizontal ‘reach’) x_c (circles) of the cough flow as a function of time. The dashed lines show the expected behaviour for a turbulent puff. The colours indicate the two models for τ_s (see Section 2.3). Note that the axes here are logarithmic. (b) Time variation of x_c plotted on linear axes.

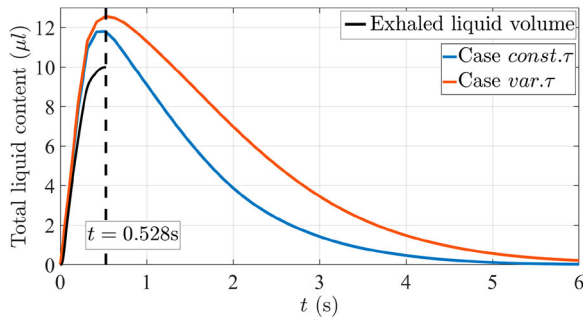


Figure 5. Time variation of the total liquid content in the cough flow for the $\text{const. } \tau$ and $\text{var. } \tau$ models.

see also Figure S5(a) in the supplementary material. Figure 4(b) also shows a comparison of the present results with those reported by Chong et al. (2021). As can be seen, there is a good match between the x_c variation from Chong et al. (2021) and that for the $\text{var. } \tau$ model from the present study.

Figure 5 shows the total liquid–water content within the cough volume as a function of time. The black solid line indicates the liquid volume exhaled at the orifice; a total of 10 μl is expelled over the cough duration of 0.528 s. The total liquid contents for both the models show an initial increase and exhibit consistently larger

values than the exhaled liquid content (Figure 5). At the end of the cough duration, there is an increment in liquid volume of 18% and 25%, respectively, for the $\text{const. } \tau$ and $\text{var. } \tau$ models compared to the total exhaled liquid. This implies that there is an initial condensation of the water vapour expelled from the orifice, which can be attributed to supersaturation, causing an increase in the liquid volume. In this connection, Chong et al. (2021) found that higher saturation and lower temperature conditions of the ambient (90% and 20°C) were favourable for longer survival of droplets in their simulations, again due to condensation of the supersaturated water vapour in the cough. We have replicated the same ambient conditions here and, therefore, the trend in Figure 5 indicates that we have been able to accurately capture the physical effects of supersaturation using the present scheme. After $t = 0.528$ s, the liquid volume starts decreasing as the droplets evaporate in the sub-saturated environment created due to the dilution of the cough flow by the entrained ambient air (Figure 5). The evolution of the saturation field within the cough flow will be presented in some detail in Section 3.2.

Comparing the const. τ and var. τ models in relation to Figure 5 shows that the const. τ model considerably under-predicts the liquid content as compared to that for the var. τ model at a given time instant (especially for $t > 0.528$). Alternatively, liquid water takes a longer time to evaporate down to a specified level for the var. τ model compared to that for the const. τ model. This is due to an increase in the value of $\tilde{\tau}_c$ (implying longer evaporation time scales) for the former model as a result of a decrease in the number density and droplet size with time (Equation (11)); for the latter model $\tilde{\tau}_c$ is kept fixed giving a constant evaporation time scale. We therefore expect the var. τ model to be more realistic in simulating the thermodynamics of phase change in mild cough flows and present more results for this case in the next section. A few additional results for the const. τ model are presented in Figures S4 and S5 in the supplementary material.

Figure 5 gives us useful information about the time it takes for most of the expelled liquid to get evaporated. We find that it takes about 10 times the cough duration for the liquid content to drop to less than 5% of its initial value for the var. τ model (and 7.5 times the cough duration for the const. τ model; Figure 5). During this time, the streamwise distance travelled by the cough flow is about 1.3–1.5 m (Figure 4(b)). Liquid droplets in such flows are thus long-lived. (We note, however, that we have assumed an initially monodisperse droplet size distribution.) It is expected that for a stronger cough the lifetimes and the distances travelled would be even larger.

3.2. Flow Evolution and Thermodynamics for the var. τ Model

Figure 6(a) shows the variation of the Stokes number for the cough flow, $St = \tau_p/\tau_f$, as a function of time. The droplet response (or relaxation) time is calculated as $\tau_p = \rho_l D_o^2 / 18 \mu_g$, for the initial droplet diameter ($D_o = 2a_o$) of 10 μm ; here μ_g is the dynamic viscosity of air. The flow time scale τ_f is typically written as the ratio of a flow length scale to a flow velocity scale. We use three different measures for τ_f based on different choices of velocity and time scales. A natural choice is to use the *mean* cough-flow velocity u_{mean} (averaged over $V(t)$; see Figure 4(a)) and the *mean* width of the cough-flow σ_{mean} defined in

Equation (28), where the mean is taken over x .

$$\frac{\pi}{4} \sigma_{\text{mean}}^2 = \text{mean} \left[\int_{y,z} dy dz \right] \quad \text{for } \tilde{r}_v > 0.91. \quad (28)$$

For this measure of τ_f , which represents a large-eddy turnover time, the Stokes number is found to be negligibly small, dropping from about 5×10^{-4} to less than 10^{-5} as time progresses (Figure 6(a)). The second choice for τ_f is taken to be the Kolmogorov time scale, which is the smallest time scale in the turbulence cascade, given as $\sqrt{\nu \sigma_{\text{mean}} / u_{\text{mean}}^3}$ (Rosti et al. 2021). This is based on the estimate of energy dissipation as $\sim u_{\text{mean}}^3 / \sigma_{\text{mean}}$. The Stokes number calculated from this measure of τ_f shows somewhat higher values than that based on the large-eddy time, but the absolute values of St are still fairly small, ranging from 10^{-2} to 10^{-4} (Figure 6(a)).

The third measure of τ_f is obtained based on the maximum velocity (u_{max}) and the minimum flow width (σ_{min}) of the cough flow as the velocity and length scales; σ_{min} is defined in Equation (29). This results in the maximum possible values for the Stokes number at a given time instant, shown in Figure 6(a) as dashed lines. Note that these St values are not necessarily realised by the cough liquid droplets but represent an upper bound that is not likely to be exceeded by any droplet. As seen from Figure 6(a), the upper bound on St has a value of 10^{-1} at $t = 0$ but drops rapidly to 10^{-2} after the end of cough duration (~ 0.5) s and continues to drop to reach values less than 10^{-3} at $t = 6$ s. Thus even the largest possible estimates of St within the cough flow are less than 10^{-1} .

$$\frac{\pi}{4} \sigma_{\text{min}}^2 = \min_x \left[\int_{y,z} dy dz \right] \quad \text{for } \tilde{r}_v > 0.91. \quad (29)$$

This exercise shows that for droplets of the order of 10 μm in diameter and with flow parameters representing a mild cough, the Stokes numbers within the flow domain are sufficiently small ($\ll 1$). As shown in section S5 of the supplementary material, the Stokes drag term is negligible in this limit and the gravitational settling effects are small over the duration of the simulation. This provides a support to our earlier premise (Section 2.2) that the droplets in our simulation follow the streamlines of the flow and that the effect of slip velocity can be neglected. Note that even for a somewhat larger droplet diameter of, say, 30 μm , the Stokes numbers based on the Kolmogorov time

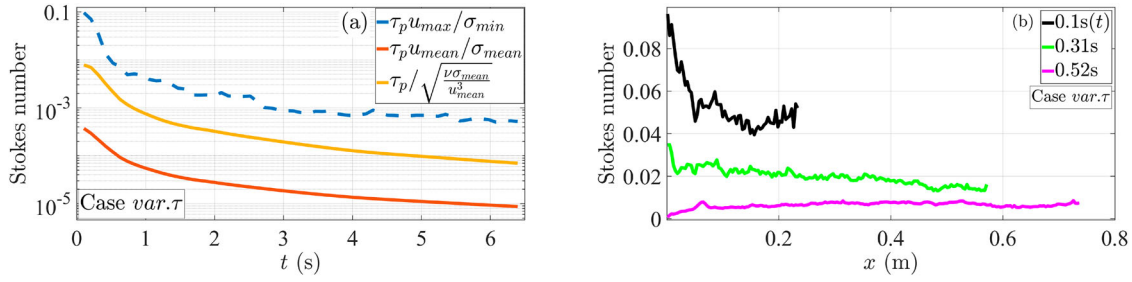


Figure 6. (a) Variation of the Stokes number for the cough flow ($St = \tau_p/\tau_f$) with time, where τ_p and τ_f are the droplet-response and flow time scales respectively, with three different measures for τ_f . The initial droplet diameter is $2a_o = 10 \mu\text{m}$. (b) Streamwise variation of the local Stokes number for three time instants.

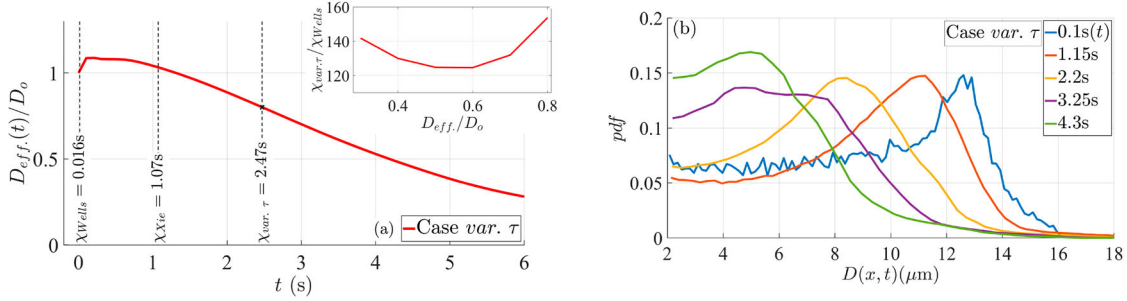


Figure 7. (a) Time variation of the effective droplet diameter D_{eff}/D_o ; D_o being the initial diameter. The inset compares the droplet lifetimes in the present simulation with predictions from Wells (1934) for different shrinkage criteria. (b) Comparison of probability distribution function (*pdf*) for droplet diameters at different times instants. The mean droplet size decreases as the liquid evaporates.

scale can be expected to be of the order of 10^{-2} – 10^{-3} , which are $\ll 1$. Thus the present formulation can, in principle, be applied to somewhat larger droplets sizes as well.

Figure 6(b) shows the streamwise variation of the Stokes number at three time instants of the cough duration: 0.1 s which is close the peak cough flow rate, 0.52 s which is close to the end of the cough duration, and 0.31 s which is an intermediate time instant (Figure 1(b)). For these cases, the local τ_f (i.e. at a given x) is calculated based on the local width of the flow and the maximum streamwise velocity at that x . At $t = 0.1$ s, St values are somewhat higher (6×10^{-2} – 10^{-1}) for $x < 0.05$ m but beyond this distance they are smaller. For the two later time instants St is typically of the order of 10^{-2} , providing a further support to our main premise. In this connection, it is relevant to refer to the results of Rosti et al. (2021) who carried out a numerical experiment for an initial mono-disperse droplets of $10 \mu\text{m}$ diameter, wherein simulations were carried out with and without droplet inertia. They plotted the centre of mass of the cloud of droplets (Figure 9 in Rosti et al. 2021) and found that the x location of the centre of mass was closer to the orifice when inertia was accounted for as compared to the

no-inertia case. This can be understood in relation to Figure 6(b) ($t = 0.1$ and 0.31 s), wherein droplets with higher Stokes numbers are found located closer to the orifice. If such droplets are large enough for the inertial effects to be important (say, due to much higher Re and therefore smaller τ_f in Rosti et al. 2021), the centre of mass of the resulting droplet cloud can be expected to shift towards the orifice, in comparison to the no-inertia case.

Next, we calculate the lifetimes (χ) of droplets from our simulation and compare them with the theoretical estimates of Wells (1934) and Xie et al. (2007); also see Chong et al. (2021). Towards this, we consider the total liquid content at a given time instant (Figure 5) to be consisting of N_o droplets of uniform size and calculate the effective droplet diameter D_{eff} by equating the total liquid volume to $N_o(\pi/6)D_{eff}^3$. The variation of D_{eff}/D_o with time is presented in Figure 7(a). Following Chong et al. (2021), we first calculate the 80% lifetime, i.e. the time taken by droplets to shrink to 80% of the initial diameter. This comes out to be $\chi_{var. \tau} = 2.47$ s marked in Figure 7(a). Also shown in the figure are the estimates of Wells (χ_{Wells}) and Xie et al. (χ_{Xie}) for the 80% lifetime. We find that $\chi_{var. \tau}/\chi_{Wells} = 153.4$ which is consistent with

the range 100–150 obtained for this ratio by Chong et al. (2021) in their simulations. The accurate capture of extended lifetimes of the cough droplets, vis-a-vis Wells (1934), provides a further verification to the present approach. Note that Wells (1934) derived the dependence of droplet lifetime on its size, considering an isolated droplet evaporating in an ambient whose temperature and relative humidity remain unchanged (see Section S3 in the supplementary material). Since the temperature and relative humidity experienced by droplets within the cough volume can vary considerably in space and time due to turbulence (see Figures 8 and 9 and also Chong et al. 2021), χ_{Wells} underestimates the actual droplet lifetime by two orders of magnitude. On the other hand, Xie et al. (2007) coupled the local temperature and humidity fields experienced by a single droplet to a *steady-state* jet in estimating droplet lifetime. As a result, χ_{Xie} is much larger than χ_{Wells} but still falls short of $\chi_{\text{var.}\tau}$ by a factor of 2.4 (Figure 7(a)). This points out the need to invest further modelling efforts to predict droplet lifetimes accurately for a realistic cough, which is inherently *transient* in nature.

The 80% criterion used by Chong et al. (2021) was possibly due to a short simulation time (1.2 s) used in their study. In the present work, we have run the simulation till 6 s, which allows us to determine the time taken for a droplet to shrink to about 30% of the initial diameter. We have determined droplet lifetimes for the shrinkage criterion ranging from 80% to 30% and compared them with the Wells' estimates, calculated using equation S3 in the supplementary material for these shrinkage criteria. The ratio $\chi_{\text{var.}\tau}/\chi_{\text{Wells}}$ is plotted as a function of D_{eff}/D_0 corresponding to the different shrinkage criteria; see the inset in Figure 7(a). The variation of $\chi_{\text{var.}\tau}/\chi_{\text{Wells}}$ is non-monotonic, highlighting the crucial role played by the effective temperature and relative-humidity fields surrounding droplets in determining the evaporation rate for a given droplet size. Note that the ratio $\chi_{\text{var.}\tau}/\chi_{\text{Wells}}$ remains of the order ~ 100 , consistent with previous results.

As discussed in Section 2.3, the *var.τ* model enables us to calculate the local diameter $D(\mathbf{x}, t)$ based on the local $\tilde{r}_l(\mathbf{x}, t)$ distribution (Equation (12)). Figure 7b shows the probability density function (*pdf*) of the droplets (for $D(\mathbf{x}, t) > 2 \mu\text{m}$) at different time instants. A range of droplet sizes up to a maximum of $18 \mu\text{m}$ is present, all of which originate from the

mono-disperse initial droplet diameter of $10 \mu\text{m}$. For $t = 0.1$ and 1.15 s, the *pdf* peaks at diameters greater than $10 \mu\text{m}$ indicating that, for small times, the dominant phase-change process is the condensation of water vapour due to supersaturation. This is apparent from Figure 8(a), which shows that the maximum relative humidity within the cough flow much exceeds $RH = 1$ for $t < 2$ s. The presence of supersaturation is the primary reason why $D_{\text{eff}}/D_0 > 1$ for small times (Figure 7(a)) and why the droplets have extended lifetimes as seen earlier; see Chong et al. (2021). Referring back to Figure 7(b), for $t \geq 2.2$ s, the peak in the *pdf* shifts to droplets smaller than $10 \mu\text{m}$ suggesting that droplet evaporation becomes the dominant phase-change process, due to an increased sub-saturation of the environment; see Figure 8(b).

Figure 8(a) shows the maximum temperature (T_{max}) and relative humidity ($(r_v/r_s)_{\text{max}}$) present within the cough volume; the corresponding mean values ($T_{\text{mean}}, (r_v/r_s)_{\text{mean}}$), averaged over $V(t)$, are plotted in Figure 8(b). Due to the presence of large condensation rates during the cough ($t < 0.528$ s), some regions undergo sufficient heating to raise the maximum temperature slightly above 34°C , which is the orifice temperature (Figure 8(a)). After the cough ends, T_{max} declines at a rapid rate primarily due to the entrainment of ambient fluid (Diwan et al. 2020); there is also a contribution from the droplet evaporation which acts as a sink for temperature. On the other hand, the maximum and mean relative humidity decreases much more slowly (Figure 8(a,b)), as the evaporation acts as a source of water vapour. Due to the decrease in temperature (requiring less water vapour for saturation) and continued evaporation, there always exists a region in the flow which is near saturation condition; i.e. $(r_v/r_s)_{\text{max}} \approx 1$ even for $t > 2.5$ s (Figure 8(a)). On average, however, the cough fluid is sub-saturated for the entire simulation time as seen in Figure 8(b). Rosti et al. (2021) have argued that the mean saturation in a moist puff should decay like $t^{-3/4}$. They observed the $t^{-3/4}$ behaviour for an extended time duration (0.1–100 s) due to a smaller value (60%) of the ambient relative humidity used in their simulations, which is not expected to lead to supersaturation (Chong et al. 2021). In the present case, the $t^{-3/4}$ variation for $(r_v/r_s)_{\text{mean}}$ is apparent after $t = 3$ s (Figure 8(b)), presumably because of the presence of supersaturation in some parts of the flow at earlier time instants. Interestingly, the start of this

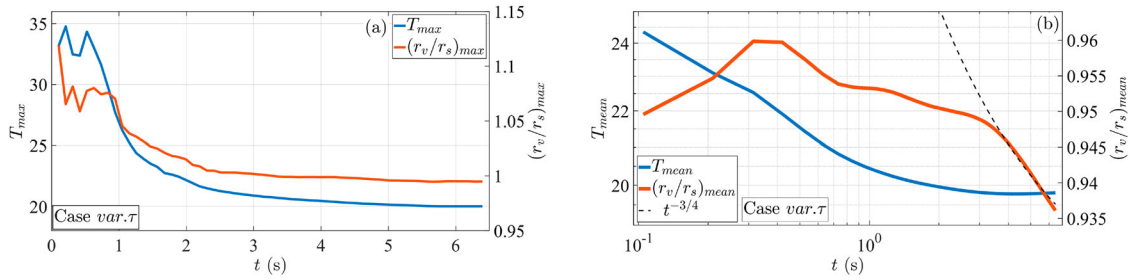


Figure 8. Time variation of (a) maximum and (b) mean temperature and relative humidity within the cough volume.

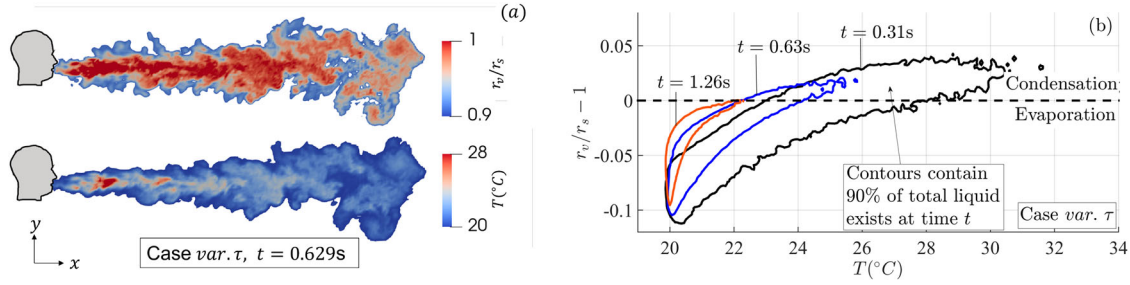


Figure 9. (a) Contours of relative humidity (top) and temperature (bottom) at time $t = 0.629$ s. (b) Contours wrapping 90% of total liquid content at time t plotted on a local supersaturation $(r_v/r_s - 1)$ vs. temperature (T) diagram. The plot shows the saturation-temperature conditions at which most of the liquid content (or droplets) exists at any time t .

power-law decay coincides with the location where T_{mean} nearly reaches a constant value close to the ambient temperature. One may expect that the $t^{-3/4}$ variation would continue if the present simulation was run for a longer time. A similar behaviour of $(r_v/r_s)_{\text{mean}}$ is also observed for the const. τ case, as shown in Figure S4 in the supplementary material.

In the following, we present detailed distributions of the various flow and thermodynamic quantities, which is the real strength of the present computational scheme. Figure 9(a) shows contour plots of the relative humidity and temperature at $t = 0.629$ s, i.e. just after the cough ends; both exhibit a considerable degree of

inhomogeneity due to turbulence. At this time instant, the region within the core of the cough flow is supersaturated (indicated by saturated red colour in the colour map; Figure 9(a)), whereas the region near the edges of the flow is in a sub-saturated state; see also Chong et al. (2021). Thus both condensation and evaporation take place simultaneously within the cough volume. This is seen more clearly in Figure 9(b) which presents the evolution of the phase-change characteristics on a supersaturation $(r_v/r_s - 1)$ vs. temperature plot. This plot is obtained as follows. The total liquid content present within the cough volume ($\tilde{r}_v > 0.91$) at a given time instant is distributed over $250 \times$

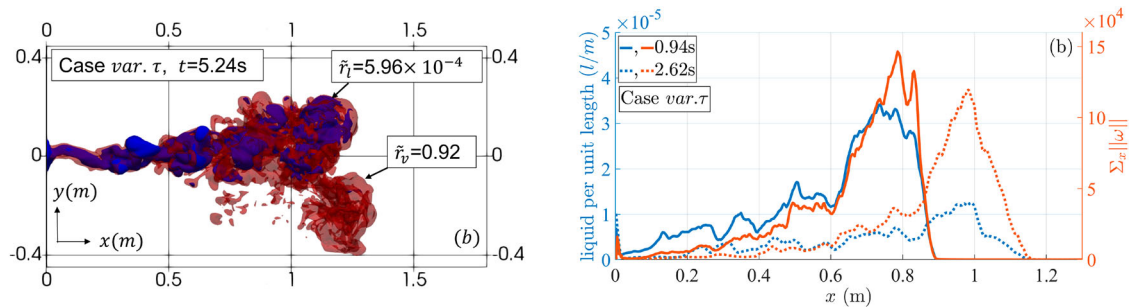


Figure 10. (a) Iso-surfaces of the vapour mixing ratio at $\tilde{r}_v = 0.92$ (semi-transparent red) and the liquid mixing ratio (blue) at $\tilde{r}_l = 5.96 \times 10^{-4}$. (b) The axial distribution of liquid content per unit length and total vorticity at a given x location (summed over the y - z plane). These plots for the var. τ model can be compared with those for the const. τ model presented in Figure S5 of the supplementary material. In particular, Figure S5(a) shows that the chunk separated from the main flow for the const. τ model moves to greater streamwise distances than that seen here for the var. τ model.

250 bins of the saturation-temperature grid and is summed over each bin. A specific contour level is chosen such that 90% of the total liquid present at that time instant lies inside that contour. Such contours are plotted in Figure 9(b) for three time instants. For example, at time $t = 0.31$ s, 90% of the liquid content (or droplets) experience the supersaturation-temperature conditions that lie inside the black curve in Figure 9(b). The dashed line at $r_v/r_s = 1$ (Figure 9(b)) provides a demarcation between condensation (due to supersaturation) and evaporation (due to sub-saturation). These can be mapped onto the regions in physical space affected by condensation/evaporation by making contour plots such as the one presented in Figure 9(a). At $t = 0.31$ s in Figure 9(b), a considerable region is subjected to supersaturation causing an increase in liquid content, consistent with the previous discussion in relation to Figures 7 and 8. As time increases, the contour contracts more rapidly along the temperature axis as compared to the saturation axis. Furthermore, the effect of supersaturation (i.e. $r_v/r_s > 1$) diminishes rapidly with time so that beyond at $t = 1.26$ s, the liquid content is expected to decay by evaporation; see Figure 5. The saturation-temperature diagram in Figure 9(b) can serve as a useful tool in visualising the thermodynamics of phase change in an evolving cough flow.

An iso-surface of water vapour with $\tilde{r}_v = 0.92$ at $t = 5.24$ s is shown in Figure 10(a). The slightly higher value of $\tilde{r}_v = 0.92$ chosen here (as compared to 0.91 used earlier as a threshold for determining $V(t)$) enables discerning certain flow features better, especially the chunk of fluid which is about to separate from the main cough flow at this time instant seen in Figure 10(a). This feature has been reported by Liu et al. (2021), who found that the separated portion of the cough flow carries droplets with it and travels at a faster speed than the main flow, potentially resulting in a faster spread of infection. Figure 10(a) also shows an iso-surface of liquid water (blue) with $\tilde{r}_l = 5.96 \times 10^{-4}$, which is visualised through the semi-transparent vapour contour (red). The vapour is seen to wrap around the liquid content and shield it from the ambient conditions, providing a visual confirmation to the inference drawn in Chong et al. (2021) that this vapour shielding effect contributes to the extended droplet lifetimes by providing an elevated local relative-humidity field. Note that the liquid mixing ratio of $\tilde{r}_l = 5.96 \times 10^{-4}$ corresponds to the

droplet diameter of $4 \mu\text{m}$ (Equation (12)); droplets of larger size are expected to be present within the central region of the cough flow.

Figure 10(b) presents the liquid content per unit length and the absolute vorticity magnitude (summed over the y - z plane) as a function of x for two time instants. It is seen that the majority of liquid is concentrated within the ‘head’ of the cough flow, which is also the region where vorticity magnitude is large. In fact the streamwise distributions of the liquid concentration and vorticity are similar to each other (Figure 10(b)). The large vorticity present within the cough head suggests the presence of a toroidal vortex which can trap liquid droplets within it. Since such vortex structures are known to maintain their identity over long distances, we may expect the trapped liquid droplets to travel with them and contribute to the long-range transmission of pathogens; see also Liu et al. (2021). The interaction between the liquid content and vorticity fields represents an important aspect of the dynamics of a moist puff, and is being investigated further.

3.3. Advantages and Limitations of the Present Approach

The coarse-graining of liquid droplets into an Eulerian liquid field is conceptually simpler and computationally easier to implement as compared to the Eulerian-Lagrangian solvers which track individual droplets (Rosti et al. 2021; Fabregat et al. 2021; Ng et al. 2021). For example, the Eulerian field approximation supports specification of any profile of liquid content at the orifice as a function of y , z and t . Especially, when the number of droplets in a cough becomes large, Lagrangian tracking can become computationally expensive. To illustrate this point, ideally, a comparison of Eulerian and Lagrangian treatments should be done with the same solver. However, our solver does not yet handle Lagrangian droplets, and most Lagrangian particle tracking studies in the literature (e.g. Chong et al. 2021; Liu et al. 2021; Ng et al. 2021) do not report the data on utilised computational resources. Yet, a careful comparison of the computational resource utilised in the present simulation is done with the available computational-resource data from the recent study by Fabregat et al. (2021) on the DNS of cough flow. We find that the computational cost for the present Eulerian-Eulerian solver is

about 31 times smaller as compared to the Lagrangian-Eulerian solver of Fabregat et al. (2021) when solving for the full set of governing equations. When applied to the computation of scalars (including particles in Fabregat et al. 2021) alone, the current approach is 65 times less expensive than that in Fabregat et al. (2021). A detailed discussion on this exercise is provided in section S4 in the supplementary material.

The number of droplets used in the simulation of Fabregat et al. (2021) is 1.932×10^5 (consisting of seven sizes for the initial droplet diameter between 4 and $256 \mu\text{m}$), whereas the DNS by Rosti et al. (2021) and Ng et al. (2021) use much less number of droplets, equal to 5000 (in the size range $10\text{--}1000 \mu\text{m}$). On the other hand, the equivalent number of droplets (of initial diameter $10 \mu\text{m}$) in the present simulation is $\sim 2 \times 10^7$. This corresponds to a droplet concentration of $\sim 3 \times 10^4 \text{ cm}^{-3}$ (in terms of the expelled cough volume), which is relevant for realistic coughs with maximum droplet diameters of $10\text{--}20 \mu\text{m}$; see Bourouiba (2021a). The present approach is well suited for such situations.

From the point of view of epidemiological modelling, an important input needed is the probability of infection to a susceptible person standing a few feet away from an infected person (Domino 2021; Chaudhuri, Basu, and Saha 2020). This probability can be calculated from the dose of virus-laden cough fluid to the susceptible person. This is another area where simulation of the kind presented here will be of value. For example, the present cough flow reaches an axial distance of about 5 ft at the end of 6 s (Figure 4(b)) and the total liquid content reaching a person at this distance can be readily determined from the results reported here (Figure 10(b)).

The limitations of the present approach should also be noted. Firstly, the use of the extended one-moment scheme implemented here requires a closure assumption relating the local droplet number density and the local droplet size. Our choice for this closure for the var. τ model, Equation (11), is to assume that the number density of droplets is uniform in the cough volume. Secondly, our approach works for an initial mono-disperse distribution of droplets released from the orifice, whereas respiratory events are known to produce a range of droplet sizes, as discussed above. Thirdly, we do not incorporate droplet inertia and settling effects and therefore preclude large-sized droplets, with higher Stokes numbers, from our

analysis; the analysis also precludes the long-time evolution of small droplets (see section S5 in supplementary material). Finally, we implicitly assume that there are no aerosol particles (or condensation nuclei) in the ambient air, which may not always be true.

Some of these limitations can be overcome, to varying degrees, by introducing additional considerations. A scalar transport equation may be solved for (an) additional moment(s) of the droplet size distribution to obtain its distribution in space and time (Beck and Watkins 2002). The droplet inertia and gravitational settling can be introduced (within the liquid field approximation) for larger droplets with small but finite Stokes numbers using Equation (4) above. Moreover, additional liquid water scalars representing different initial droplet sizes could be used, in analogy with multiple hydrometeor classes in simulations of atmospheric flows (e.g. Hernandez-Duenas et al. 2013), although at the cost of simplicity. A development of the present solver along some of the lines mentioned here is being carried out.

A further limitation of the solver is its simple geometry; real-life geometries are rarely cuboidal (Shao et al. 2021). This limitation may be overcome using volume penalisation (e.g. Ravichandran and Wettlaufer 2020), such that solid regions of complex shapes may be incorporated in the domain. The relatively small time step used in our explicit time-stepping permits the use of a small penalisation parameter, allowing the physics of flow around objects of complicated shapes to be adequately captured. Along with these practical domain settings, the evolution of cough droplets can be analysed in practical time settings which can span from tens of seconds to tens of minutes, provided the field approximation to droplet distribution continues to hold. As discussed in Section 2.2 above and in section S5 of the supplementary material, for large times, the decreasing Stokes number is compensated by a much larger increase in the non-dimensional gravity term, thereby making the gravitational settling velocity to be of the same order as the fluid velocity in the absence of any background ventilation. We plan to incorporate this effect in our solver along the lines done in Ravichandran and Narasimha (2020), wherein the same basic solver (*Megha-5*) has been used for simulating a mammatus cloud.

Despite the computational efficiency of the solver and the chosen Eulerian treatment of droplets, DNS

remains much more computationally expensive than other model-based approaches. For example, simulating the flow in a domain of size $3 \times 2^2 \text{ m}^3$ (a typical elevator) for about 30 s would require 1.75 million core-hours at the present resolution, which would be much higher for Lagrangian-based solvers. This suggests the need for better subgrid models for thermodynamics, which requires careful direct numerical simulations (like the one presented here).

4. Conclusion

We have used a computational approach (that may be called the extended one-moment scheme) for simulating moist cough flows, that uses an Eulerian field approximation for liquid droplets, which are advected by fluid streamlines. A closure model is proposed for the time scale of evaporation ($\tilde{\tau}_c$), which is a crucial parameter for the thermodynamics of phase change. The model considers the droplet density to be uniform in space (but varying in time) and the droplet radius a function of space and time. This model (called the var. τ model) is compared with the const. τ model, in which $\tilde{\tau}_c$ is kept constant. We find that the liquid content within the cough flow takes much longer to evaporate for the var. τ model, as compared to that for the const. τ model, due to a gradual increase in $\tilde{\tau}_c$ with time for the former, caused by dilution and evaporation. The var. τ model is shown to be closer to the realistic cough flow scenarios and has been used for a detailed investigation in the context of a mild cough. The Stokes numbers associated with the initial droplet diameter of $10 \mu\text{m}$ are plotted as a function of space and time, for three different measures of the flow time scale. The Stokes number based on the Kolmogorov time scale is found to be of the order of 10^{-2} or smaller, providing a verification to our assumption that the liquid-droplet inertia is negligible over the duration of simulation and that the liquid field is carried by the local fluid velocity. A careful analysis of the evolution and thermodynamics of the cough flow has been carried out, and a comparison is made with the results available in the literature. The following aspects of the available results have been successfully reproduced.

- The mean velocity and the streamwise extent of the cough flow follow the $t^{-3/4}$ and $t^{1/4}$ variations, respectively. The mean relative humidity follows the $t^{-3/4}$ law for the latter part of the flow evolution (Rosti et al. 2021).

- The liquid field in the core of the cough flow undergoes an initial condensation followed by evaporation at later times (Chong et al. 2021). This is due to the initial supersaturation on account of a high ambient relative humidity (90%).
- The effective droplet diameter shows an extended lifetime, which is 120–150 times larger than that predicted by the Wells' model (Wells 1934); see Chong et al. (2021).
- At later time instants in the flow evolution, a chunk of fluid separates from the main cough flow and causes an increased spread of the flow in the lateral/streamwise direction (Liu et al. 2021).

This comparison provides a strong support for the utility of our proposed approach, and we have used it to obtain some new results. For the 'mild' cough simulated herein (with the initial droplet diameter of $10 \mu\text{m}$) the time taken for the liquid content to reach 5% of its initial value has been found to be about 7–10 times the cough duration. The interpretation of the liquid field in terms of local droplet sizes (for the var. τ model) has enabled us to plot a probability density function for droplet sizes and track its evolution with time. A saturation-temperature diagram has been constructed at different time instants, which shows that the temperature of the cough flow decreases with time more rapidly than the relative humidity, thereby promoting conditions of supersaturation close to the orifice. Finally, a portion of the liquid content is shown to be trapped within the head of the cough flow, which is also a region of high vorticity and is therefore likely to survive over longer distances from the orifice. We believe the present approach is well suited to study the long-range transport of small droplets in a cough flow (after inclusion of the gravitational settling effects), which is responsible for the airborne transmission of the COVID-19 type pathogens. Our results can also provide useful inputs for calculating infection probabilities (Singhal, Ravichandran, Govindarajan, et al. 2021), in the context of epidemiological modelling.

Acknowledgments

The present simulations have been carried out at the Super-computer Education and Research Centre at the Indian Institute of Science, Bengaluru. SSD acknowledges support from Indian Institute of Science, Bengaluru, towards running the

simulations. The authors thank anonymous referees whose suggestions have helped improve the quality of the paper.

Data availability statement

The data that support the findings of this study are available on request from the corresponding author.

Disclosure statement

No potential conflict of interest was reported by the author(s).

Funding

SR is supported through the Swedish Research Council [grant number 638-2013-9243].

ORCID

Rohit Singhal  <http://orcid.org/0000-0002-0687-6930>
 S. Ravichandran  <http://orcid.org/0000-0001-9299-7570>
 Sourabh S. Diwan  <http://orcid.org/0000-0002-9190-7403>

References

- Abkarian, Manouk, Simon Mendez, Nan Xue, Fan Yang, and Howard A. Stone. 2020. "Speech Can Produce Jet-like Transport Relevant to Asymptomatic Spreading of Virus." *Proceedings of the National Academy of Sciences* 117 (41): 25237–25245.
- Asadi, Sima, Nicole Bouvier, Anthony S. Wexler, and William D. Ristenpart. 2020. "The Coronavirus Pandemic and Aerosols: Does Covid-19 Transmit Via Expiratory Particles?" *Aerosol Science and Technology* 54 (6): 635–638.
- Beck, J. C., and A. P. Watkins. 2002. "On the Development of Spray Submodels Based on Droplet Size Moments." *Journal of Computational Physics* 182 (2): 586–621.
- Bohren, Craig F., and Bruce A. Albrecht. 2000. *Atmospheric Thermodynamics*.
- Bourouiba, Lydia. 2020. "Turbulent Gas Clouds and Respiratory Pathogen Emissions: Potential Implications for Reducing Transmission of COVID-19." *JAMA* 323 (18): 1837–1838.
- Bourouiba, Lydia. 2021a. "Fluid Dynamics of Respiratory Infectious Diseases." *Annual Review of Biomedical Engineering* 23: 547–577.
- Bourouiba, Lydia. 2021b. "The Fluid Dynamics of Disease Transmission." *Annual Review of Fluid Mechanics* 53 (1): 473–508.
- Bourouiba, Lydia, Eline Dehandschoewercker, and John W. M. Bush. 2014. "Violent Expiratory Events: on Coughing and Sneezing." *Journal of Fluid Mechanics* 745: 537–563.
- Chao, C. Y. H., M. P. Wan, L. Morawska, G. R. Johnson, Z. D. Ristovski, M. Hargreaves, K. Mengersen, et al. 2009. "Characterization of Expiration Air Jets and Droplet Size Distributions Immediately At the Mouth Opening." *Journal of Aerosol Science* 40 (2): 122–133.
- Chaudhuri, Swetaprovo, Saptarshi Basu, and Abhishek Saha. 2020. "Analyzing the Dominant SARS-CoV-2 Transmission Routes Toward An Ab Initio Disease Spread Model." *Physics of Fluids* 32 (12): 123306.
- Chen, C., and Bin Zhao. 2010. "Some Questions on Dispersion of Human Exhaled Droplets in Ventilation Room: Answers From Numerical Investigation." *Indoor Air* 20 (2): 95–111.
- Chong, Kai Leong, Chong Shen Ng, Naoki Hori, Rui Yang, Roberto Verzicco, and Detlef Lohse. 2021. "Extended Lifetime of Respiratory Droplets in a Turbulent Vapor Puff and Its Implications on Airborne Disease Transmission." *Physical Review Letters* 126: 034502.
- Dbouk, Talib, and Dimitris Drikakis. 2020. "On Coughing and Airborne Droplet Transmission to Humans." *Physics of Fluids* 32 (5): 053310.
- Diwan, Sourabh S., S. Ravichandran, Rama Govindarajan, and Roddam Narasimha. 2020. "Understanding Transmission Dynamics of Covid-19-type Infections by Direct Numerical Simulations of Cough/sneeze Flows." *Transactions of the Indian National Academy of Engineering* 5: 255–261.
- Domino, Stefan P. 2021. "A Case Study on Pathogen Transport, Deposition, Evaporation and Transmission: Linking High-fidelity Computational Fluid Dynamics Simulations to Probability of Infection." *International Journal of Computational Fluid Dynamics* 323: 1–15.
- Duguid, J. P. 1946. "The Size and the Duration of Air-carriage of Respiratory Droplets and Droplet-nuclei." *Journal of Hygiene* 44 (6): 471–479.
- Fabregat, Alexandre, Ferran Gisbert, Anton Vernet, Som Dutta, Ketan Mittal, and Jordi Pallarès. 2021. "Direct Numerical Simulation of the Turbulent Flow Generated During a Violent Expiratory Event." *Physics of Fluids* 33 (3): 035122.
- Feng, Yu, Thierry Marchal, Ted Sperry, and Hang Yi. 2020. "Influence of Wind and Relative Humidity on the Social Distancing Effectiveness to Prevent Covid-19 Airborne Transmission: A Numerical Study." *Journal of Aerosol Science* 147: 105585.
- Grabowski, Wojciech W. 1998. "Toward Cloud Resolving Modeling of Large-scale Tropical Circulations: A Simple Cloud Microphysics Parameterization." *Journal of the Atmospheric Sciences* 55 (21): 3283–3298.
- Gupta, Jitendra K., C.-H. Lin, and Q. Chen. 2009. "Flow Dynamics and Characterization of a Cough." *Indoor Air* 19 (6): 517–525.
- Hernandez-Duenas, G., A. J. Majda, L. M. Smith, and S. N. Stechmann. 2013. "Minimal Models for Precipitating Turbulent Convection." *Journal of Fluid Mechanics* 717: 576–611.
- Hersen, Guillaume, Stéphane Moullarat, Enric Robine, Evelyne Géhin, Sandrine Corbet, Astrid Vabret, and François Freymuth. 2008. "Impact of Health on Particle Size of Exhaled Respiratory Aerosols: Case-control Study." *CLEAN - Soil, Air, Water* 36 (7): 572–577.
- Kovaszny, Leslie S. G., Hajime Fujita, and Rena L. Lee. 1975. "Unsteady Turbulent Puffs." In *International Union of Theoretical and Applied Mechanics and International Union of*

- Geodesy and Geophysics*, Vol. 18, edited by F. N. Frenkiel and R. E. Munn, 253–263. Elsevier.
- Lin, Yuh-Lang, Richard D. Farley, and Harold D. Orville. 1983. “Bulk Parameterization of the Snow Field in a Cloud Model.” *Journal of Applied Meteorology and Climatology* 22 (6): 1065–1092.
- Lindsley, William G., Jeffrey S. Reynolds, Jonathan V. Szalajda, John D. Noti, and Donald H. Beezhold. 2013. “A Cough Aerosol Simulator for the Study of Disease Transmission by Human Cough-generated Aerosols.” *Aerosol Science and Technology* 47 (8): 937–944.
- Liu, K., M. Allahyari, J. Salinas, N. Zgheib, and S. Balachandar. 2021. “Investigation of Theoretical Scaling Laws Using Large Eddy Simulations for Airborne Spreading of Viral Contagion From Sneezing and Coughing.” *Physics of Fluids* 33 (6): 063318.
- Maxey, Martin R., and James J. Riley. 1983. “Equation of Motion for a Small Rigid Sphere in a Nonuniform Flow.” *The Physics of Fluids* 26 (4): 883–889.
- Mittal, Rajat, Rui Ni, and Jung-Hee Seo. 2020. “The Flow Physics of COVID-19.” *Journal of Fluid Mechanics* 894: Article number - F2. doi:10.1017/jfm.2020.330
- Moin, Parviz, and Krishnan Mahesh. 1998. “Direct Numerical Simulation: a Tool in Turbulence Research.” *Annual Review of Fluid Mechanics* 30 (1): 539–578.
- Monchaux, Romain, Mickael Bourgoin, and Alain Cartellier. 2012. “Analyzing Preferential Concentration and Clustering of Inertial Particles in Turbulence.” *International Journal of Multiphase Flow* 40: 1–18.
- Morawska, Lidia, and Junji Cao. 2020. “Airborne Transmission of SARS-CoV-2: The World Should Face the Reality.” *Environment International* 139: 105730.
- Morawska, L., G. R. Johnson, Z. D. Ristovski, Megan Hargreaves, Kerrie Mengersen, Shay Corbett, Christopher Yu Hang Chao, Yuguo Li, and David Katoshevski. 2009. “Size Distribution and Sites of Origin of Droplets Expelled From the Human Respiratory Tract During Expiratory Activities.” *Journal of Aerosol Science* 40 (3): 256–269.
- Murphy, Daniel M., and Thomas Koop. 2005. “Review of the Vapour Pressures of Ice and Supercooled Water for Atmospheric Applications.” *Quarterly Journal of the Royal Meteorological Society: A Journal of the Atmospheric Sciences, Applied Meteorology and Physical Oceanography* 131 (608): 1539–1565.
- Ng, Chong Shen, Kai Leong Chong, Rui Yang, Mogeng Li, Roberto Verzicco, and Detlef Lohse. 2021. “Growth of Respiratory Droplets in Cold and Humid Air.” *Physical Review Fluids* 6 (5): 054303.
- Qian, H., and Y. Li. 2010. “Removal of Exhaled Particles by Ventilation and Deposition in a Multibed Airborne Infection Isolation Room.” *Indoor Air* 20 (4): 284–297.
- Ravichandran, S., Eckart Meiburg, and Rama Govindarajan. 2020. “Mammatus Cloud Formation by Settling and Evaporation.” *Journal of Fluid Mechanics* 899: A27.
- Ravichandran, S., and Roddam Narasimha. 2020. “Non-precipitating Shallow Cumulus Clouds: Theory and Direct Numerical Simulation.” Preprint arXiv:2004.09631.
- Ravichandran, S., and John S. Wettlaufer. 2020. “Transient Convective Spin-up Dynamics.” *Journal of Fluid Mechanics* 897: A24. doi:10.1017/jfm.2020.387
- Rosti, M. E., M. Cavaola, S. Olivieri, A. Seminara, and A. Mazzi. 2021. “Turbulence Role in the Fate of Virus-containing Droplets in Violent Expiratory Events.” *Physical Review Research* 3: 013091.
- Scorer, Robert S. 1957. “Experiments on Convection of Isolated Masses of Buoyant Fluid.” *Journal of Fluid Mechanics* 2 (6): 583–594.
- Shao, Siyao, Dezhi Zhou, Ruichen He, Jiaqi Li, Shufan Zou, Kevin Mallery, Santosh Kumar, Suo Yang, and Jiarong Hong. 2021. “Risk Assessment of Airborne Transmission of COVID-19 by Asymptomatic Individuals Under Different Practical Settings.” *Journal of Aerosol Science* 151: 105661.
- Singhal, Rohit, S. Ravichandran, Sourabh S. Diwan, and Garry L. Brown. 2021. “Reynolds Stress Gradient and Vorticity Fluxes in Axisymmetric Turbulent Jet and Plume.” In *Proceedings of 16th Asian Congress of Fluid Mechanics*, edited by L. Venkatakrishnan, Sekhar Majumdar, Ganesh Subramanian, G. S. Bhat, Ratul Dasgupta and Jaywant Arakeri, Bangalore. Singapore: Springer.
- Singhal, Rohit, S. Ravichandran, Rama Govindarajan, and Sourabh S. Diwan. 2021. “Virus transmission by aerosol transport during short conversations.” Preprint arXiv:2103.16415.
- Somsen, G. Aernout, Cees van Rijn, Stefan Kooij, Reinout A. Bem, and Daniel Bonn. 2020. “Small Droplet Aerosols in Poorly Ventilated Spaces and SARS-CoV-2 Transmission.” *The Lancet Respiratory Medicine* 8 (7): 658–659.
- Stadnytskyi, Valentyn, Christina E. Bax, Adriaan Bax, and Philip Anfinrud. 2020. “The Airborne Lifetime of Small Speech Droplets and Their Potential Importance in SARS-CoV-2 Transmission.” *Proceedings of the National Academy of Sciences* 117 (22): 11875–11877.
- Wells, W. F. 1934. “Droplets and Droplets Nuclei.” *American Journal of Epidemiology* 20 (3): 611–618.
- Xie, X., Y. Li, A. T. Chwang, P. L. Ho, and W. H. Seto. 2007. “How Far Droplets Can Move in Indoor Environments—revisiting the Wells Evaporation-falling Curve.” *Indoor Air* 17 (3): 211–225.
- Yang, Shinhao, Grace W. M. Lee, Cheng-Min Chen, Chih-Cheng Wu, and Kuo-Pin Yu. 2007. “The Size and Concentration of Droplets Generated by Coughing in Human Subjects.” *Journal of Aerosol Medicine* 20 (4): 484–494.
- Yoshimoto, Hiroshi, and Susumu Goto. 2007. “Self-similar Clustering of Inertial Particles in Homogeneous Turbulence.” *Journal of Fluid Mechanics* 577: 275–286.
- Zayas, Gustavo, Ming C. Chiang, Eric Wong, Fred MacDonald, Carlos F. Lange, Ambikaipakan Senthilselvan, and Malcolm King. 2012. “Cough Aerosol in Healthy Participants: Fundamental Knowledge to Optimize Droplet-spread Infectious Respiratory Disease Management.” *BMC Pulmonary Medicine* 12 (1): 1–12.
- Zhao, Bin, Zhao Zhang, and Xianting Li. 2005. “Numerical Study of the Transport of Droplets Or Particles Generated by Respiratory System Indoors.” *Building and Environment* 40 (8): 1032–1039.